Spectral functions of quantum dots in the integer and fractional quantum Hall regime

Arkadiusz Wójs* and Pawel Hawrylak
Institute for Microstructural Sciences, National Research Council of Canada, Ottawa, Canada K1A 0R6
(Received 25 February 1997)

The one- and two-particle spectral functions of quantum Hall droplets are studied for filling factors $2 \geqslant \nu \geqslant 1/3$ using exact diagonalization techniques for up to ten electrons. The spectral functions describe the electron addition and subtraction spectra, coherent resonant tunneling, and Raman-scattering cross section. They reflect the magnetic-field-induced spin and charge transitions in the ground state of quantum Hall droplets. [S0163-1829(97)07428-6]

I. INTRODUCTION

A laterally confined two-dimensional electron gas in a strong magnetic field forms a quantum Hall droplet.[1–3] The number of electrons per flux quanta penetrating the droplet determines the filling factor. Increasing the magnetic field drives the quantum Hall droplet of interacting electrons through a series of ground states with decreasing filling factor. In the filling factor regime $2 \geqslant \nu \geqslant 1$, the ground state is characterized by oscillations of the total spin.[4–7] For the filling factor $\nu \leqslant 1$ the ground state is characterized by oscillations of the total angular momentum.[1] For the filling factor $\nu = 1$ the droplet is expected to represent a chiral Fermi liquid, while for fractional filling factors the low-energy charge excitations of the edges of the droplet are expected to be described by the chiral Luttinger-liquid theory.[8–10] Some aspects of this interesting behavior have already been probed experimentally by capacitance,[11–13] transport,[14–17] and interband magneto-optical[18,19] spectroscopies. Recent work has demonstrated that Raman scattering[20–23] can directly probe charge and spin excitations of quantum dots. The understanding of these, and in particular Raman, experimental probes requires the calculation of the response of a many-electron system to the external perturbation introduced in these experiments. Because of the strong electron correlations nonperturbative calculations, such as exact-diagonalization methods, are a useful tool[6,7,13,21,24,25] in studying one- and two-particle spectral functions in the integer and fractional quantum Hall regimes. The electron and hole one-particle spectral functions describe the processes of adding and subtracting electrons to/from the droplet, and therefore describe the charging of the dot and hence capacitance and incoherent transport. The two-particle spectral functions describe charge and spin excitations of the droplet for a fixed number of electrons. These functions define the inelastic light scattering cross section and the coherent transport through a quantum dot.[17]

In this paper we numerically analyze the spectral functions of a finite droplet of a few ($\leqslant 10$) electrons both in the integer and fractional quantum Hall regimes. The spectral functions are related to the magnetic-field-induced transitions between different ground states of the droplet, from the spin transitions in the integer regime, through the chiral Fermi-liquid behavior at $\nu = 1$, to the chiral Luttinger-liquid behavior at fractional filling factors.

II. MODEL

We study the system of N quasi-two-dimensional electrons in a strong magnetic field B, and parabolic confining potential with characteristic frequency ω_N.[13]

The single-particle Hamiltonian corresponds to a pair of harmonic oscillators with energies $\varepsilon_{mn} = \Omega_+(n+\frac{1}{2}) + \Omega_-(m+\frac{1}{2})$, where $\Omega_\pm = \frac{1}{2}(\sqrt{\omega_c^2 + 4\omega_N^2} \pm \omega_c)$, and $\omega_c = eB/m^*c$ is the cyclotron frequency and m^* is the effective mass. The magnetic length is $l_0 = 1/\sqrt{m^*\omega_c}$ and the effective magnetic length in the presence of confinement is $l_{\rm eff} = l_0/(1+4\omega_N^2/\omega_c^2)^{1/4}$. The orbital angular momentum of the state $|m,n\rangle$ is $m-n$. We shall concentrate here on strong magnetic fields, with the electrons confined to the lowest Landau level, and omit further the index n. The Zeeman energy is $g\mu_B B\sigma$, where σ is the electron's spin, g is the effective Landé g factor, and μ_B is the Bohr magneton.

The Hamiltonian of the many-electron system can be written in the form

$$H = \sum_{m\sigma} (\varepsilon_m + g\mu_B B\sigma) c^\dagger_{m\sigma} c_{m\sigma} + \frac{1}{2} \sum_{\substack{m_1 m_2 m_3 m_4 \\ \sigma' \sigma}} \langle m_1 m_2 | V | m_3 m_4 \rangle c^\dagger_{m_1\sigma} c^\dagger_{m_2\sigma'} c_{m_3\sigma'} c_{m_4\sigma}. \tag{1}$$

The operators $c^\dagger_{m\sigma}$ and $c_{m\sigma}$ create and annihilate an electron in the single-particle state with spin σ and angular momentum m. The first term in Eq. (1) is the single-particle energy, and the second term describes the electron-electron Coulomb scattering, with the two-body matrix elements defined in Ref. 27. The Coulomb energy is measured in units of exchange energy $E_0 = {\rm Ry}\sqrt{2\pi} a_B / l_{\rm eff}$, where Ry is the effective Rydberg, and a_B is the effective Bohr radius.

Hamiltonian H conserves the number of electrons N, the total angular momentum R, the total spin S, and the component of the total spin along the magnetic field S_z. The N-electron basis states spanning the Hilbert spaces with defined (R,S_z) can be constructed as the noninteracting configurations $|m_1\sigma_1, \ldots, m_N\sigma_N\rangle = c^\dagger_{m_1\sigma_1} \ldots c^\dagger_{m_N\sigma_N} |{\rm vac}\rangle$, where $|{\rm vac}\rangle$ denotes a vacuum. The filling factor for a given state can be defined as the ratio of the total angular momen-

 © 1997 The American Physical Society

tum of the compact state $R=(N-1)\times N/2$ to the actual angular momentum R. Since for the parabolic confinement the noninteracting Hamiltonian is a constant within each subspace (R,S_z), only the diagonalization of the interaction part V is necessary. Since the Coulomb interaction is invariant under rotation of the total spin S, degenerate states corresponding to the same total spin appear in different subspaces S_z. It is useful here to define *compact* configurations with the lowest R for a given S_z.[7,26] These compact configurations $|C^k_{N-k}\rangle=|0\downarrow,\ldots,(N-k-1)\downarrow;0\uparrow,\ldots,(k-1)\uparrow\rangle$ are the only states in their Hilbert spaces, and therefore they are the *exact* eigenstates of the interacting Hamiltonian H. The Hartree-Fock calculations[16,26] are restricted only to these compact states.

For a given N the Hilbert space (R,S,S_z) containing the ground state is a result of the competition between the Zeeman, kinetic, and interaction energies. These energies are controlled by the magnetic field, confinement, and effective g factor. The magnetic field drives the system through a sequence of ground states with increasing angular momentum R, i.e. decreasing filling factor ν. The following states are among the ground states in the following sequence: (i) the spin-unpolarized $(S=0)$ compact state $|C^{N/2}_{N/2}\rangle$, corresponding to the filling factor $\nu=2$; (ii) the spin-polarized $(S=\frac{1}{2}N)$ compact state $|C^0_N\rangle$, with $\nu=1$; and (iii) the spin-polarized highly correlated state with $\nu=\frac{1}{3}$. In the following we shall study the properties of the system in this range of the filling factor $(\nu=2-\frac{1}{3})$, or, alternatively, in the corresponding range of the magnetic field, confinement strength, or electron density. The states with the filling factor $\nu>1$ and $\nu<1$ can be viewed as created through the spin and charge excitations of the compact $\nu=1$ droplet, respectively.

A. Spin excitations

In order to describe spin excitations of the system, we can take advantage of the mapping between the two-spin electron system and the spinless electron-hole system.[28,29] We identify a spin-up electron with an electron and a removed spin-down electron with a hole: $a^\dagger_m=c^\dagger_{m\uparrow}$ and $b^\dagger_k=c_{k\downarrow}$. The spin-flip excitation $c^\dagger_{m\uparrow}c_{k\downarrow}$ corresponds to creating a pair of quasiparticles (i.e., a spin exciton): $a^\dagger_m b^\dagger_k$.

With the operators $a^\dagger$ and $b^\dagger$ the Hamiltonian H [Eq. (1)] can be transformed into the form

$$\begin{aligned}H-\mathcal{E}_N=&\sum_m\left(\varepsilon_m+\frac{1}{2}g\mu_B+\Sigma^H_m\right)a^\dagger_m a_m\\&-\sum_k\left(\varepsilon_k-\frac{1}{2}g\mu_B+\Sigma^{\mathrm{HF}}_k\right)b^\dagger_k b_k\\&+\tfrac{1}{2}\sum_{m_1m_2m_3m_4}\langle m_1m_2|V|m_3m_4\rangle a^\dagger_{m_1}a^\dagger_{m_2}a_{m_3}a_{m_4}\\&+\tfrac{1}{2}\sum_{k_1k_2k_3k_4}\langle k_1k_2|V|k_3k_4\rangle b^\dagger_{k_1}b^\dagger_{k_2}b_{k_3}b_{k_4}\\&-\sum_{m_1k_2k_3m_4}\langle m_1k_3|V|k_2m_4\rangle a^\dagger_{m_1}b^\dagger_{k_2}b_{k_3}a_{m_4},\end{aligned}\tag{2}$$

where $\mathcal{E}_N$ is the energy of the state $|C^0_N\rangle$, $\Sigma^H_m=\Sigma^{N-1}_{i=0}\langle mi|V|im\rangle$ and $\Sigma^{\mathrm{HF}}_k=\Sigma^{N-1}_{i=0}(\langle ki|V|ik\rangle-\langle ki|V|ki\rangle)$ are the Hartree and Hartree-Fock self-energies, respectively.

For fixed N, the number of spin-excitons n and their total angular momentum r are a pair of good quantum numbers, replacing S_z and R. Hamiltonian (2) was diagonalized numerically in each Hilbert space (n,r). The Hilbert spaces labeled by (n,r) were constructed from states of noninteracting spin-excitons: $|m_1,\ldots,m_n;k_1,\ldots,k_n\rangle=a^\dagger_{m_1}\ldots a^\dagger_{m_n}b^\dagger_{k_1}\ldots b^\dagger_{k_n}|C^0_N\rangle$. The computations including all possible spin states (S,S_z) were carried out for up to $N=10$.

B. Charge excitations

In analogy with spin excitations, the charge excitations of the $\nu=1$ droplet can be viewed as creation of pairs (charge excitons) of quasielectrons and quasiholes ($c^\dagger_{l\downarrow}c_{m\downarrow}$, with $l\geqslant N$ and $m<N$). The transformation to the electron-hole Hamiltonian, described in detail in Ref. 19, is more complicated in this case, since the Coulomb interaction does not conserve the number of charge excitons n. Thus the total angular momentum R is the only nontrivial good quantum number. However, for $n\ll N$ the scattering processes leading to change in n are inefficient, and the ground states can be approximated by configurations with fixed n (cf. Ref. 19). We have studied states with a limited number of charge excitons $(n\leqslant 3)$ for fairly large droplets (up to $N=30$) in the vicinity of the filling factor $\nu=1$. For filling factors around $\nu=\frac{1}{3}$, computations were performed in the complete basis of noninteracting N-electron configurations, and hence were limited to $N\leqslant 7$. $N=6$ is the minimum number of electrons which shows features characteristic of the incompressible liquid.[3]

C. Spectral functions

The pair of one-particle spectral functions are the electron and hole Green's functions $A^+_{m\sigma}$ and $A^-_{m\sigma}$. $A^+_{m\sigma}(\omega)$ $[A^-_{m\sigma}(\omega)]$ gives the probability to add (subtract) an electron with angular momentum m, spin σ, and energy ω, to (from) the droplet:

$$A^\pm_{m\sigma}(\omega)=\sum_f|\langle f_{N\pm1}|c^\pm_{m\sigma}|i_N\rangle|^2\delta(|\mathcal{E}^f_{N\pm1}-\mathcal{E}^i_N|-\omega).\tag{3}$$

The $|i_N\rangle$ and $|f_{N\pm1}\rangle$ are the initial N-electron and final $(N\pm1)$-electron states, respectively, with energies $\mathcal{E}^i_N$ and $\mathcal{E}^f_{N\pm1}$. The two operators $c^\pm$ create and annihilate electrons in the single-particle states labeled by m and σ. This pair of functions describes the charging process changing the number of electrons in the droplet. It describes the capacitance spectroscopy and incoherent transport.

The two-particle spectral functions describe the coupling of the external perturbation to charge and spin excitations of the system for a fixed number of electrons N. They are of the form

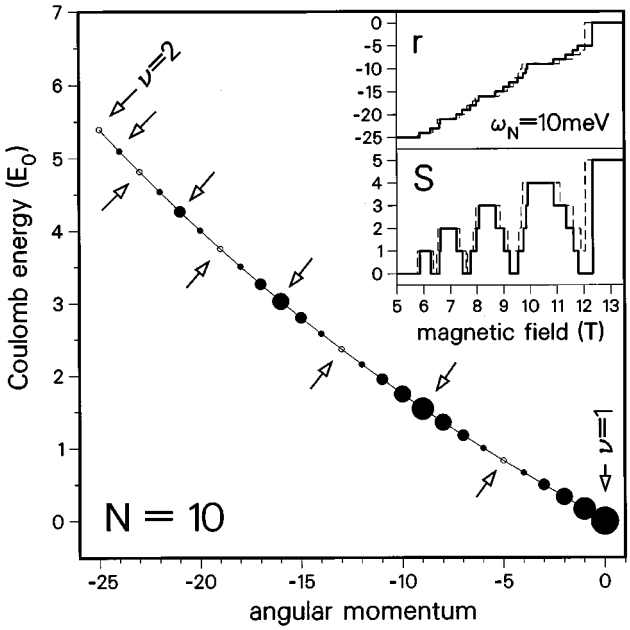

FIG. 1. The Coulomb energy of ten electrons as a function of angular momentum (data on both axes measured from a $\nu=1$ state), between filling factors $\nu=2$ and 1. Sizes of black dots reflect total spin S. Arrows above (below) the curve indicate the compact (zero-spin) states. Insets: magnetic-field evolution of angular momentum (r) and spin (S) for the parabolic confinement of $\omega_N=10$ meV; solid (dashed lines)—result without (with) including the Zeeman splitting.

$$A(\omega)=\sum_f \left| \left\langle f \left| \sum_{\substack{m_1\sigma_1\\ m_2\sigma_2}} a^{m_1\sigma_1}_{m_2\sigma_2} c^{\dagger}_{m_1\sigma_1} c_{m_2\sigma_2} \right| i \right\rangle \right|^2 \times \delta(|\mathcal{E}^f-\mathcal{E}^i|-\omega), \tag{4}$$

where $|i\rangle$ and $|f\rangle$ are the initial and final electronic states with the energies $\mathcal{E}^i$ and $\mathcal{E}^f$, and the information about the form of the perturbation is hidden in the coefficients a. These functions define, e.g., the Raman-scattering cross section and the coherent transport through a quantum dot.[17]

III. INTEGER QUANTUM HALL REGIME

We calculated the energy spectra for up to $N=10$ electrons in the subspaces corresponding to the filling factor $1\leqslant\nu\leqslant 2$. The minimum Coulomb energy of ten electrons within each subspace R is plotted in Fig. 1, and the total spin of the corresponding eigenstates is given by the size of black dots. Both energy and angular momenta are measured from the values appropriate for the $\nu=1$ state: $R=45$ and $E=9.937E_0$. The dependence of the energy on R is very regular, and by varying the strength of confinement versus interaction (e.g. by changing the magnetic field) the system is driven from $\nu=2$ to 1 through a series of intermediate states with increasing R (i.e., increasing area). However, an interesting observation[5–7] is the oscillation of the total spin S as a function of R, and, consequently, of the filling factor. The highly correlated states with $S=0$, indicated by arrows, appear between the neighbouring compact states C^k_{N-k} with the maximum allowed spin for a given R. The spin-depolarized state at, e.g., $R=-5$ corresponds to an electron with flipped spin which has been removed from the edge and placed in between the edge and the center of the droplet. This minority-spin electron creates spin excitons. The number of spin excitons depends on the Zeeman energy. In the limit of Landé factor $g=0$, half of the electrons flip their spins, and the lowest-energy configuration corresponds to the total spin $S=0$. Unlike the single spin-exciton configuration with this angular momentum the correlated states with $S=0$ correspond to smeared excess spin and charge over the entire droplet.

The dependence of angular momentum and spin of the ground state on the magnetic field for the effective parabolic confinement of $\omega_N=10$ meV has been presented in the insets. The material parameters used here are appropriate for GaAs: $m^*=0.067m_e$, $a_B=98$ Å, $g\mu_B=0.03$ meV/T, and Rydberg Ry$=5.93$ meV. The solid lines show the result without Zeeman energy, and the dashed line includes Zeeman energy. The sharp depolarization at $B=12.5$ T (the transition occurs from the maximum allowed spin $S=\frac{1}{2}N$ at $\nu=1$ directly to the minimum allowed spin $S=0$ at $\nu\sim 1^+$) reflects the almost linear dependence of the Coulomb energy on angular momentum between $R=0$ and $R=-\frac{1}{2}N$. For $N=10$ the dependence is sublinear, but the exact shape depends on N. The Coulomb energy is also a linear function of the total spin S, or a number of spin excitons n. The consecutive $\frac{1}{2}N$ spin excitons, each of them carrying angular momentum -1, are created in a $\nu=1$ droplet with the same energy, and effectively form a noninteracting gas.[7] For sufficiently large Zeeman energy the correlated low-S states can be pushed up, so that the transition between $\nu=2$ and 1 occurs through a series of compact states C^k_{N-k}.

A. One-particle spectral functions

The depolarization of the droplet occurring during the transition between neighboring compact states C^k_{N-k} and C^{k+1}_{N-k-1}, has a dramatic effect on the spectral functions. In Fig. 2 we show the evolution with the magnetic field of the pair of Green's functions calculated for $N=6$ electrons. The top frame shows the spin-$\downarrow$ (majority-spin) addition spectrum $A^+_\downarrow=\Sigma_m A^+_{m\downarrow}$, and the bottom frame the spin-$\uparrow$ (minority-spin) subtraction spectrum $A^-_\uparrow=\Sigma_m A^-_{m\uparrow}$. The effective confinement is $\omega_N=7$ meV, and the $C^1_{N-1}\rightarrow C^0_N$ transition occurs at the magnetic fields $B\approx 4$–5 T. The area of the circles is proportional to the intensity of individual transitions. The transition energy ω is measured from the energy of charging an empty dot with the first electron. The dashed lines show the bottom (top) edge of the addition (subtraction) spectrum, i.e. the chemical potentials of five and six electrons. At certain magnetic fields the ground states of N and $N\pm 1$ electrons are not coupled through the addition and/or subtraction operator due to the spin selection rules, and only transitions to the excited final states are allowed.[6] The vertical lines mark the magnetic field-induced transitions in the initial ground state, their angular momenta R, and spins S indicated in each sector as (R,S).

In compact states the addition spectrum of a majority-spin electron is very simple, since an electron can be added only to the completely empty states outside the droplet. The spectra are dominated by a pair of strong transitions correspond-

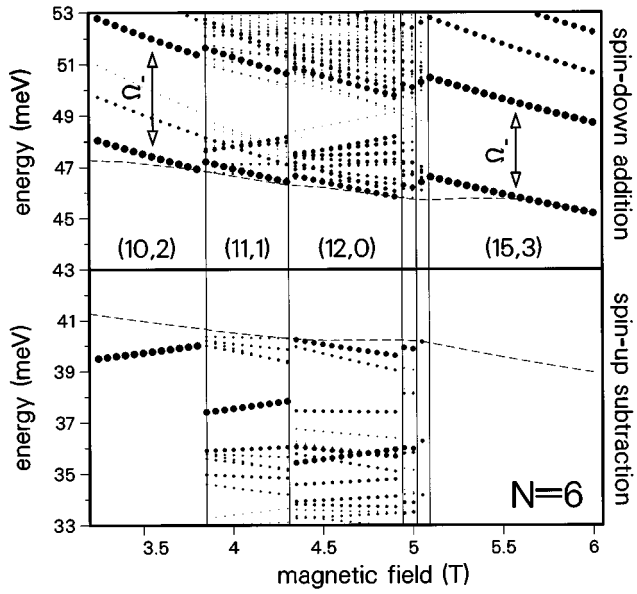

FIG. 2. The magnetic-field evolution of the one-electron Green's functions of six electrons, between filling factors $\nu=2$ and 1. Top frame: spin-$\downarrow$ addition spectrum; bottom frame: spin-$\uparrow$ subtraction spectrum. The effective confinement is $\omega_N=7$ meV. The areas of the circles give the transition intensities. The energy on the vertical axes does not include the cyclotron energy $\frac{1}{2}\omega_c$. The dashed lines show the chemical potentials. The vertical lines separate initial ground states with indicated angular momenta and spins (R,S).

ing to the final compact and excited state, different from the compact state by the center-of-mass excitation. For example, at $\nu=1$ in the initial state ($B\sim5.5$ T), these two final states are the single-particle configurations, obtained from a compact initial state $|i_N\rangle$ by adding an electron to a definite orbital: $c_N^\dagger|i_N\rangle$ and $c_{N+1}^\dagger|i_N\rangle$. Their intensity is therefore equal to unity, and the spacing between them is the center-of-mass single particle excitation energy $\Omega_-\sim4$ meV.

Conversely, for the low-spin correlated states at $B\sim4$–5 T, a large number of low-energy transitions appears in the addition spectrum. Because the initial state is no longer spin polarized we can add a majority-spin electron to the interior of the droplet. The Hilbert subspace coupled to the initial ground state through an addition operator (the subspace with low total spin) contains many more low-energy states than that coupled to an initial compact, large-spin state. Hence there are a number of allowed transitions to excited final states with the excitation energies below the noninteracting gap Ω_-.

The spin depolarization between compact and correlated ground states has even more dramatic effect on the minority-spin subtraction spectrum. The $\nu=1$ state C_N^0 is polarized with spin-$\downarrow$, and we cannot subtract a spin-$\uparrow$ electron. In the state C_{N-1}^1 there is only one spin-$\uparrow$ electron, occupying a single-particle state (with $m=0$), and hence only one transition is allowed to the final compact state C_{N-1}^0. However, in the depolarized states there is a number of spin-$\uparrow$ electrons smeared over many single-particle states that can be removed, leaving the $N-1$ electrons in a distinct spectrum of final states.

Summarizing, there are two main features in the one-particle spectral functions signaling the transitions: (i) oscillations of the lowest (highest) energy line in the addition (subtraction) spectrum (a sharp jump of the addition edge that would appear at the $C_N^0\rightarrow C_{N-1}^1$ transition is though significantly reduced due to the presence of intermediate correlated states), and (ii) appearance of a large number of additional, almost degenerate transitions when the initial ground state is a low-spin correlated state, compared to very simple spectra when the initial state is compact. This should be observable in the temperature dependence of the tunneling and capacitance spectra.

B. Two-particle spectral functions

As an illustration of the two-particle spectral functions, we calculate the dynamical structure factor $S(q,\omega)$. $S(q,\omega)$ is related to the electronic Raman spectrum.[20,21] It has been shown that at large wave-vector transfer q (q^{-1} of the order of the size of the droplet) the Raman spectrum measures the charge and spin excitations of interacting electrons,[20,21] and hence can serve as a tool in the experimental investigation of electrons in the quantum Hall droplets.

The Raman cross section I, proportional to the imaginary part of the dynamical structure factor, can be calculated by applying the Fermi's golden rule to the single-particle time-dependent perturbation $V(t)\sim MA_iA_se^{i\mathbf{qr}}\mathbf{e}^{-i\omega t}+$c.c., where $\mathbf{A}_i$ and $\mathbf{A}_s$ are the vector potentials of the incident and scattered light, and the resonance condition with the valence band is hidden in M:[21,22]

$$I(q,\omega)=\sum_f\ |\langle f|\sum_{\substack{m_1\sigma_1\\ m_2\sigma_2}} a_{\sigma_1\sigma_2}\varrho_{m_1m_2}(q)c_{m_1\sigma_1}^\dagger c_{m_2\sigma_2}|i\rangle|^2 \times\delta(|\mathcal{E}^f-\mathcal{E}^i|-\omega), \tag{5}$$

where $|i\rangle$ and $|f\rangle$ are the initial (ground) and final electronic states, respectively, with corresponding energies $\mathcal{E}^i$ and $\mathcal{E}^f$, and $\varrho_{m_1m_2}(q)=\langle m_1|e^{i\mathbf{qr}}|m_2\rangle$. The spin matrix element $a_{\sigma_1\sigma_2}$ contains $\langle\sigma_1|\sigma^+|\sigma_2\rangle=\delta_{\sigma_1,\uparrow}\delta_{\sigma_2,\downarrow}$, $\langle\sigma_1|\sigma^-|\sigma_2\rangle=\delta_{\sigma_1,\downarrow}\delta_{\sigma_2,\uparrow}$, $\langle\sigma_1|\sigma_z|\sigma_2\rangle=\sigma_1\delta_{\sigma_1,\sigma_2}$, and $\langle\sigma_1|\hat{\mathbf{1}}|\sigma_2\rangle=\delta_{\sigma_1,\sigma_2}$, depending on the orientation of $\mathbf{A}_i$, $\mathbf{A}_s$, and $\mathbf{B}$, and on the resonance condition with the valence band.

In Fig. 3 we show the magnetic-field evolution of the Raman spectra calculated for six electrons. The top frame shows the charge-density excitation spectrum, corresponding to the $e^{i\mathbf{q}\cdot\mathbf{r}}$ coupling, and the bottom frame shows the spin-flip excitation spectrum, with the $\sigma^-e^{i\mathbf{q}\cdot\mathbf{r}}$ coupling (a minority-spin electron is flipped: $|S_z|\rightarrow|S_z|+1$). All the parameters and notation are the same as in Fig. 2, and the wave-vector transfer is $q=10^6$ cm^{-1}.

The charge-density operator connects the Hilbert subspaces with different angular momenta R but the same total spin. The magnetic field induces changes in the total spin of the ground state. The implied level crossing is therefore between states with different total spin. Hence there is always a finite gap in the spectrum. At $\nu=1$ the spectrum corresponds to the center-of-mass excitations and the edge magnetorotons[19,26] with energies above Ω_-; at higher filling factors new low-energy transitions appear. At $q=10^6$

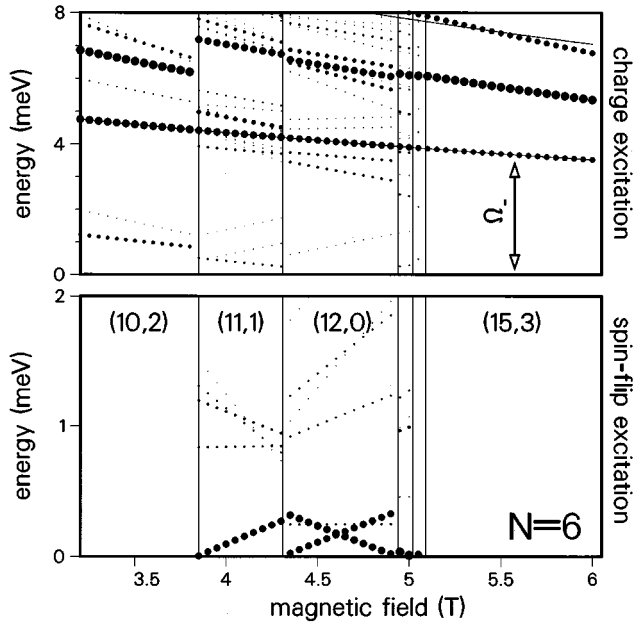

FIG. 3. The magnetic-field evolution of the Raman spectra of six electrons, between filling factors $\nu=2$ and 1. Top frame: charge-excitation spectrum; bottom frame: spin-flip-excitation spectrum. The effective confinement is $\omega_N=7$ meV. The areas of the circles give the transition intensities. The vertical lines separate initial ground states with indicated angular momenta and spins (R,S).

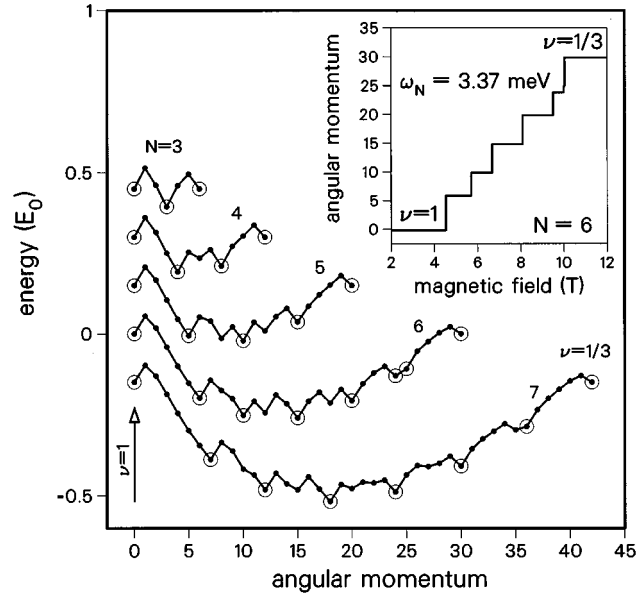

FIG. 4. The ground-state energies of $N=3$–7 electrons within each angular-momentum subspace, between the filling factors $\nu=1$ and $\frac{1}{3}$. Angular momenta are measured from the $\nu=1$ states. Circles mark the ''magic'' states. The magnetic field for each N is chosen such that the energies of the $\nu=1$ and $\frac{1}{3}$ states are equal. The curves for different N are vertically shifted. Inset: magnetic-field evolution of the angular momentum of six electrons for the effective confinement of $\omega_N=3.37$ meV.

cm^{-1} these transitions are rather weak compared to the edge magnetoroton and center-of-mass excitation, but they become dominant at higher q.

Transitions between the compact and correlated low-spin states are clearly visible in the minority-spin-flip spectrum. At $\nu=1$ there are no spin-$\uparrow$ electrons, and the spectrum is empty. In the next compact state (C^1_{N-1}) the transition requires a large angular momentum transfer ($\Delta R \geqslant N-1$), i.e., large q, in order to produce a visible peak in the spectrum. Conversely, when the initial ground state has a low total spin, a strong low-energy transition between this state and a neighboring ground state ($\Delta S=1$ and $\Delta R=\pm 1$) becomes possible. In particular, transitions from the correlated states to their compact neighbors are allowed: $(11,1)\rightarrow(10,2)$ and $(14,2)\rightarrow(15,3)$, appearing with a high intensity at zero energy when a reconstruction of a compact state occurs.

IV. FRACTIONAL QUANTUM HALL REGIME

The reconstruction of a compact spin-polarized state at $\nu=1$ toward lower filling factors occurs through the introduction of quasiholes into the bulk of the droplet and deposition of quasielectrons at the edge.[2,8,19,26] For small, parabolically confined droplets ($N\leqslant 11$) the first transition occurs with the angular momenta of the pairs $r=N$. A number of consecutive holes is created in the central orbitals with $m=0,1,\ldots$), and the series of reconstructed states resembles rings with increasing radius. For larger droplets ($N\geqslant 12$) the reconstructed states correspond to a droplet with a ring of holes. Further transitions go through strongly correlated states with selected values of angular momenta, ''magic'' states. These magic states can be assigned a filling factor and they evolve into incompressible liquid states of the fractional quantum Hall effect.

In Fig. 4 we plot the ground-state energy of $N=3$–7 electrons in each angular-momentum subspace between the filling factor $\nu=2$ and $\frac{1}{3}$. Circles mark the energies of ''magic'' states. The magnetic field and confinement for each N are chosen such that for each N the energies of the $\nu=1$ and $\frac{1}{3}$ states are equal. The vertical axis gives the energy of six electrons measured from those two states, and the curves for other N are shifted. The horizontal axis, common for all N, gives angular momentum measured from the $\nu=1$ state $r=R-\frac{1}{2}N(N-1)$.

By increasing the strength of Coulomb interaction versus the kinetic energy Ω_- (e.g., by applying the magnetic field as shown in the inset for an effective confinement of $\omega_N=3.37$ meV), the system is driven through a series of states. For $N>3$ there is a pair of sequences of states at which the downward cusps in energy appear. These are the states with angular momenta r being multiples of N and $N-1$, respectively. The series of the ground states is a result of the competition between the states from the two sequences, and e.g., for $N=6$ it is $r=6$, 10, 15, 20, 24, 25, and 30. The two sequences meet at $\nu=1$ $[r=0]$ and at $\nu=\frac{1}{3}$ $[r=N(N-1)]$, and these two ground states are more stable than the intermediate ones.

A. One-particle spectral functions

Let us now examine how the transitions between ''magic'' states are reflected in the spectral functions. The magnetic field evolution of the spin-$\downarrow$ addition spectra $A^+_\downarrow=\Sigma_m A^+_{m\downarrow}$, calculated for $N=3$–6 and the effective con-

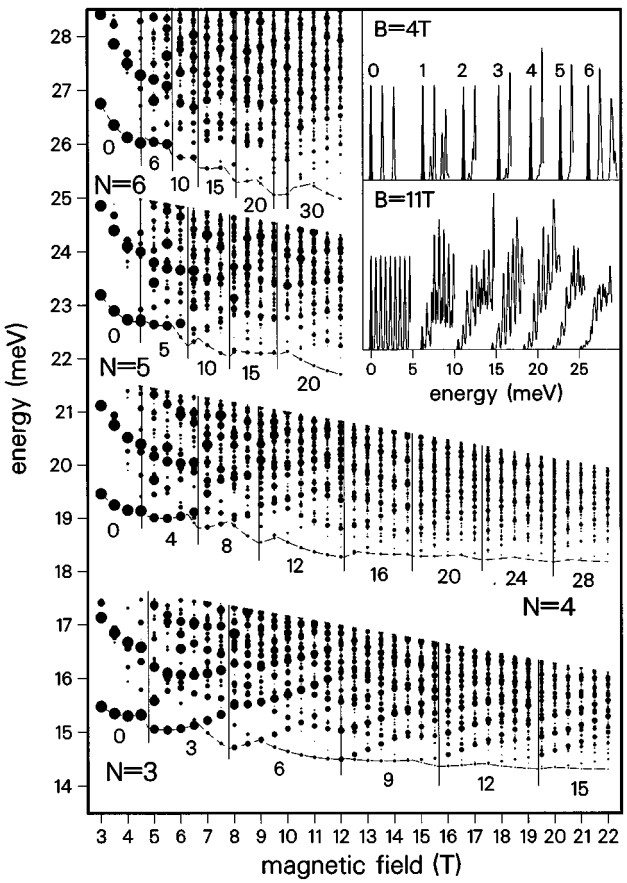

FIG. 5. The magnetic-field evolution of the addition spectra of $N=3$–6 electrons, between filling factors $\nu=1$ and $\frac{1}{3}$. The effective confinement is $\omega_N=3.37$ meV. The areas of the circles give the transition intensities. The energy on the vertical axes does not include the cyclotron energy $\frac{1}{2}\omega_c$. The dashed lines show the chemical potentials. The vertical lines separate initial ground states with indicated angular momenta (measured from the $\nu=1$ states). Inset: addition spectra for $N=0$–6 and filling factors $\nu=1$ ($B=4$ T) and $\nu=\frac{1}{3}$ ($B=11$ T). Full black peaks—transitions to the ground states.

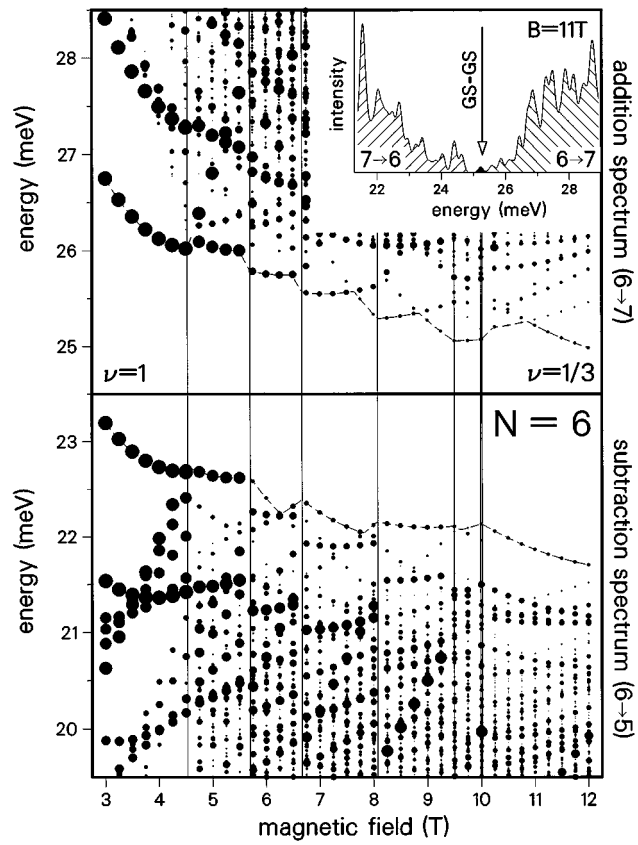

FIG. 6. The magnetic-field evolution of the one-electron Green's functions of six electrons, between filling factors $\nu=1$ and $\frac{1}{3}$. Top frame: addition spectrum; bottom frame: subtraction spectrum. The effective confinement is $\omega_N=3.37$ meV. The areas of the circles give the transition intensities. The energy on the vertical axes does not include the cyclotron energy $\frac{1}{2}\omega_c$. The dashed lines show the chemical potentials. The vertical lines separate initial ground states. Inset: addition spectrum for $N=6$ and subtraction spectrum for $N=7$, at $\nu=\frac{1}{3}$ ($B=11$ T). Full black peak—transitions between the six- and seven-electron ground states.

finement of $\omega_N=3.37$ meV, is shown in Fig. 5. Only the low-energy parts of A^+ have been shown, corresponding to the transitions to the final ground and weakly excited states. The area of the circles gives transition intensities, and the transition energy ω does not include the cyclotron energy $\frac{1}{2}\ \omega_c$. The dashed lines show the chemical potentials. The vertical lines mark the magnetic-field-induced transitions in the initial ground states, with their angular momenta r (measured from $\nu=1$ states) indicated in each sector. For example, at the field $B\sim4$ T all initial and final N-electron ground states ($N=2$–7) are compact, with $\nu=1$ [$r=0$], and for $B\sim11$ T have the same filling factor $\nu=\frac{1}{3}$ [$r=N(N-1)$]. The addition or subtraction at $B\sim4$ and 11 T occurs therefore without changing the filling factor.

A decrease of the filling factor has a strong effect on the addition spectra. The simple addition spectra at $B=4$ T ($\nu=1$) is dominated by a pair of strong transitions: to the final $\nu=1$ ground state, and to the center-of-mass excited final state, the transitions become far more complicated at higher fields. With decreasing ν we observe (i) suppression of the transitions between the initial and final ground states, and (ii) shrinking of the spacing between the neighboring low-energy transitions, measuring the excitation gap in the final system, compared to the center-of mass gap at $\nu=1$. While at $\nu=1$ the ground state (GS) can be described as a Fermi disk ($m<N$), with electrons added to or subtracted from the Fermi level with the one-particle operator $\Sigma_m c_m^{\pm}$, the suppression of the GS-GS transitions below $\nu=1$ is a strong signature of the non-Fermi liquid. This is illustrated in the inset, where for a pair of fields $B=4$ and $B=11$ T we plot the overall intensities (individual peaks broadened with Gaussians) as a function of energy. The electron numbers $N=0$–6 in the frames for $B=4$ T indicate transitions to the final ground states (black-filled peaks). Clearly, the probability of a GS-GS transition for a fixed fractional filling factor $\nu=\frac{1}{3}$ decays rapidly with the droplet size N. The GS-GS transition probability is a decreasing function of both N and ν^{-1}, and efficient adding of electrons to the fractional state of larger droplets has to occur through the excited final states. The pair of addition and subtraction spectra for $N=6$ is plotted in Fig. 6. The evolution of the subtraction spectrum with decreasing filling factor is very similar to that of an addition spectrum. The chemical potential of the finite

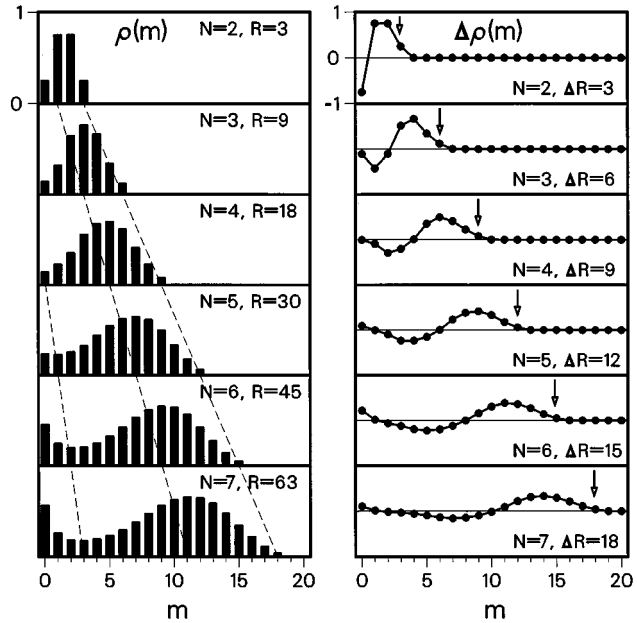

FIG. 7. Left: The occupation numbers $\varrho_N(m)$ for the magic $\nu=\frac{1}{3}$ states of $N=2$–7 electrons. Right: Differences between the occupation numbers for the neighboring $\nu=\frac{1}{3}$ states $\Delta\varrho_N(m)\equiv\varrho_N(m)-\varrho_{N-1}(m)$. Arrows show the orbitals with $m=\Delta R\equiv R_N-R_{N-1}$.

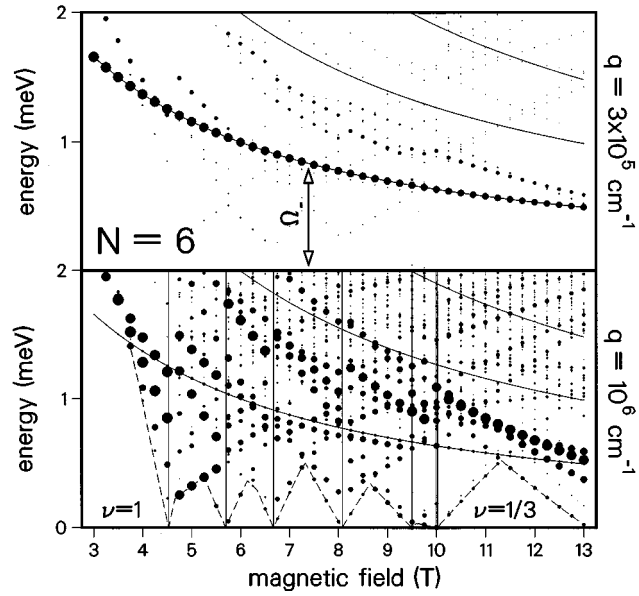

FIG. 8. The magnetic-field evolution of the Raman spectra of six electrons, between filling factors $\nu=1$ and $\frac{1}{3}$. Top frame: low wave-vector transfer ($q=3\times10^5$ cm^{-1})—dominant center-of-mass excitation; bottom frame: high wave-vector transfer ($q=10^6$ cm^{-1})—coupling to the internal-motion excitations. The effective confinement is $\omega_N=3.37$ meV. The areas of the circles give the transition intensities. The vertical lines separate initial ground states.

(incompressible) system depends on N, and the two spectra in Fig. 6 are separated by a gap.

When the N-electron droplet is in contact with a single electrode, as in capacitance experiments, the $(N+1)$st electron tunnels back and forth between the droplet and the electron. The relevant density of states corresponds to addition $(N\rightarrow N+1)$ and subtraction $(N\leftarrow N+1)$ spectra for $N=6$ and $\nu=\frac{1}{3}$. The suppression of the GS-GS tunneling and the frequency dependence of the density of states is shown in the inset to Fig. 6. The overall frequency dependence of the density of states appears to be in qualitative agreement with the chiral Luttinger liquid theory ($\approx\omega^2$).

The reason for the suppression of GS-GS transitions can be explained as follows. The difference in total angular momentum between the N and $N+1$ electron system at the same filling factor has to be absorbed by adding an electron into a single-particle orbital. This creates a final state very different from the ground state, and the corresponding overlap $\langle f|c_m^{\pm}|i\rangle$ between many-body states is very small. In the left-hand frame of Fig. 7 we show the occupations of single-particle states $\varrho_N(m)=\langle c_m^{\dagger}c_m\rangle$ for the series of ground states with $\nu=\frac{1}{3}$ and $N=2$–7. The distribution $\varrho(m)$ evolves regularly with increasing size: the positions of the edge and of the developing maxima and minima shift linearly with increasing N, as indicated by dashed lines. In the right-hand frame of Fig. 7 we show the change in the distribution due to adding or subtracting the Nth electron: $\Delta\varrho_N(m)=\varrho_N(m)-\varrho_{N-1}(m)$. The arrows show the single-particle orbitals with $m=\Delta R$, to which this electron is added with the one-particle operator $\Sigma_m c_m^{+}$.

B. Two-particle spectral functions

Let us now turn to the charge excitation spectrum in the fractional regime. In Fig. 8 we present the magnetic-field evolution of the Raman cross section calculated for six electrons, between the filling factors $\nu=1$ and $\frac{1}{3}$. The notation and parameters are the same as in Fig. 5. In the upper frame the wave-vector transfer $q=3\times10^5$ cm^{-1} is too low to excite the internal motion of electrons, and the spectrum is dominated by the center-of-mass excitation with the single-particle energy Ω_-. In the lower frame the wave-vector transfer $q=1\times10^6$ cm^{-1} is sufficient to show the excitations of interacting electrons. The lowest-energy transition follows the excitation gap of the interacting system. The gap for the filling factors $\nu=2$, 1, and $\frac{1}{3}$ is comparable to the single-particle gap Ω_-. The excitation gap collapses at magnetic-field values where the transition between the neighboring magic states takes place. The interactions make the droplet compressible.

V. CONCLUSION

We have studied the magnetic-field-induced transitions of the quantum Hall droplet, in the range of the filling factor ν covering both the integer and fractional quantum Hall regimes. Increasing magnetic field drives the droplet through the sequence of ground states with decreasing filling factor. For $2>\nu>1$ the total spin of the system oscillates as a function of the magnetic field. The ground state alternates between compact Hartree-Fock configurations with the maximum allowed spin at a given ν, and highly correlated states with zero total spin. The spin depolarization of the droplet results in a significant modification of the spectral weight in the one- and two-particle spectral functions. For a spin-polarized droplet at $\nu<1$ the sequence of ground states corresponds to a sequence of ''magic'' values of angular mo-

mentum, minimizing the electron-electron repulsion. The correlated ''magic'' states translate into fractional filling factor incompressible states. The supression of many-particle overlap matrix elements leads to a suppression of ground-state addition and subtraction spectra. The frequency dependence of the one-particle spectral function appears to be consistent with the chiral Luttinger-liquid behavior. The calculated Raman spectrum shows the closing of the excitation gap by increasing magnetic field due to the crossing of energy levels of the interacting electron system. The frequency and wave-vector dependence is, however, complicated in contrast to a simple behavior implied by bosonization theories.

ACKNOWLEDGMENTS

We thank M. R. Geller for useful discussions. A.W. acknowledges the Institute for Microstructural Sciences, NRC Canada, the KBN Grant No. PB 674/P03/96/10 for financial support, and L. Jacak for helpful discussions.

*Permanent address: Institute of Physics, Technical University of Wrocław, Wybrzeże Wyspiańskiego 27, 50-370 Wrocław, Poland.

[1] For recent reviews and references, see M. Kastner, Phys. Today **24(1)**, xxx (1993); T. Chakraborty, Comments Condens. Matter Phys. **16**, 35 (1992); R. C. Ashoori, Nature (London) **379**, 413 (1996).

[2] A. H. MacDonald, S. R. Eric Yang, and M. D. Johnson, Aust. J. Phys. **46**, 345 (1993).

[3] P. A. Maksym, Physica B **184**, 385 (1993); P. A. Maksym and T. Chakraborty, Phys. Rev. Lett. **65**, 108 (1990); P. A. Maksym and T. Chakraborty, Phys. Rev. B **45**, 1947 (1992).

[4] E. H. Rezayi, Phys. Rev. B **36**, 5454 (1987).

[5] P. Hawrylak and D. Pfannkuche, Phys. Rev. Lett. **70**, 485 (1993).

[6] J. J. Palacios, L. Martin-Moreno, G. Chiappe, E. Louis, and C. Tejedor, Phys. Rev. B **50**, 5760 (1994).

[7] J. H. Oaknin, L. Martin-Moreno, and C. Tejedor, Phys. Rev. B **54**, 16 850 (1996).

[8] X. G. Wen, Phys. Rev. B **41**, 12 838 (1990); C. de Chamon and X.-G. Wen, *ibid.* **B49**, 8227 (1994).

[9] J. M. Kinaret, Y. Meir, N. S. Wingreen, P. A. Lee, and X.-G. Wen, Phys. Rev. B **46**, 4681 (1992).

[10] J. J. Palacios and A. H. MacDonald, Phys. Rev. Lett. **76**, 118 (1996).

[11] R. C. Ashoori, H. L. Stormer, J. S. Weiner, L. N. Pfeiffer, K. W. Baldwin, and K. W. West, Phys. Rev. Lett. **71**, 613 (1993).

[12] Bo Su, V. J. Goldman, and J. E. Cunningham, Science **255**, 313 (1992).

[13] P. Hawrylak, Phys. Rev. Lett. **71**, 3347 (1993).

[14] P. L. McEuen, E. B. Foxman, J. M. Kinaret, U. Meirav, M. A. Kastner, N. S. Wingreen, and S. J. Wind, Phys. Rev. B **45**, 11 419 (1992).

[15] A. Sachrajda, R. P. Taylor, C. Dharma-Wardana, P. Zawadzki, J. A. Adams, and P. T. Coleridge, Phys. Rev. B **47**, 6811 (1993).

[16] O. Klein, S. de Chamon, D. Tang, D. M. Abusch-Magder, U. Meirav, X.-G. Wen, M. A. Kastner, and S. J. Wind, Phys. Rev. Lett. **74**, 785 (1995).

[17] P. Hawrylak, in *Proceedings XXXII Winter School of Theoretical Physics, Karpacz (Poland), 1996*, edited by Z. Petro, J. Przystawa, and K. Rapcewicz, Lecture Notes in Physics Vol. 477, (Springer Verlag, Berlin, 1997), p. 59.

[18] S. Patel, A. S. Plaut, P. Hawrylak, H. Lage, P. Grambow, D. Heitmann, K. von Klitzing, J. P. Harbison, and L. T. Florez, Solid State Commun. (to be published).

[19] P. Hawrylak, A. Wójs, and J. A. Brum, Solid State Commun. **98**, 847 (1996); Phys. Rev. B **54**, 11 397 (1996).

[20] D. J. Lockwood, P. Hawrylak, P. D. Wang, C. M. Sotomayor-Torres, A. Pinczuk, and B. S. Dennis, Phys. Rev. Lett. **77**, 354 (1996).

[21] P. Hawrylak, Solid State Commun. **93**, 915 (1995).

[22] A. O. Govorov and A. V. Chaplik, Solid State Commun. **85**, 827 (1993).

[23] R. Strentz *et al.*, Phys. Rev. Lett. **73**, 3022 (1994).

[24] Y. Hatsugai, P.-A. Bares, and X. G. Wen, Phys. Rev. Lett. **71**, 424 (1993).

[25] Song He, P. M. Platzmann, and B. I. Halperin, Phys. Rev. Lett. **71**, 777 (1993).

[26] P. Hawrylak, Phys. Rev. B **51**, 17 708 (1995).

[27] P. Hawrylak, Solid State Commun. **88**, 475 (1993).

[28] A. H. MacDonald and E. H. Rezayi, Phys. Rev. B **42**, 3224 (1990).

[29] A. Wójs and P. Hawrylak, Solid State Commun. **100**, 487 (1996); P. Hawrylak and A. Wójs, Semicond. Sci. Technol. **11**, 1516 (1996).